nature medicine

Suppressing aberrant GluN3A expression rescues synaptic and behavioral impairments in Huntington's disease models

Sonia Marco[1,12], Albert Giralt[2,12], Milos M Petrovic[1,3], Mahmoud A Pouladi[4,5], Rebeca Martínez-Turrillas[1], José Martínez-Hernández[6], Linda S Kaltenbach[7], Jesús Torres-Peraza[2], Rona K Graham[4,11], Masahiko Watanabe[8], Rafael Luján[6], Nobuki Nakanishi[9], Stuart A Lipton[9], Donald C Lo[7], Michael R Hayden[4,5,10], Jordi Alberch[2], John F Wesseling[1] & Isabel Pérez-Otaño[1]

Huntington's disease is caused by an expanded polyglutamine repeat in the huntingtin protein (HTT), but the pathophysiological sequence of events that trigger synaptic failure and neuronal loss are not fully understood. Alterations in *N*-methyl-D-aspartate (NMDA)-type glutamate receptors (NMDARs) have been implicated. Yet, it remains unclear how the HTT mutation affects NMDAR function, and direct evidence for a causative role is missing. Here we show that mutant HTT redirects an intracellular store of juvenile NMDARs containing GluN3A subunits to the surface of striatal neurons by sequestering and disrupting the subcellular localization of the endocytic adaptor PACSIN1, which is specific for GluN3A. Overexpressing GluN3A in wild-type mouse striatum mimicked the synapse loss observed in Huntington's disease mouse models, whereas genetic deletion of GluN3A prevented synapse degeneration, ameliorated motor and cognitive decline and reduced striatal atrophy and neuronal loss in the YAC128 Huntington's disease mouse model. Furthermore, GluN3A deletion corrected the abnormally enhanced NMDAR currents, which have been linked to cell death in Huntington's disease and other neurodegenerative conditions. Our findings reveal an early pathogenic role of GluN3A dysregulation in Huntington's disease and suggest that therapies targeting GluN3A or pathogenic HTT-PACSIN1 interactions might prevent or delay disease progression.

Huntington's disease is a progressive neurodegenerative disorder with severe motor, cognitive and psychiatric disturbances that is caused by expansion of a polyglutamine repeat within the N-terminal region of HTT. Mutant HTT (mHTT) accumulates as an oligomeric species and aggregates throughout neuronal soma and dendrites[1–3], triggering synaptic failure and loss that is later followed by the death of subsets of striatal and cortical neurons. Limitations in understanding the mechanisms that underlie HTT toxicity, especially at the early stages of disease, have been a major obstacle to finding a treatment.

A prevalent hypothesis is that mHTT engages in aberrant protein interactions, interfering with the function of key cellular components. But HTT interacts with a large network of proteins[4,5], and discerning which interactions are pathogenic has been difficult. Nevertheless, a prominent group of HTT interactors comprises proteins involved in clathrin-mediated endocytosis[6,7], pointing toward altered protein trafficking as a key pathological mechanism.

One of these interactors, PACSIN1 (also called syndapin 1), works as an endocytic adaptor for neuronal NMDARs[8]. NMDARs have crucial roles in remodeling and maintaining excitatory synapses, and their activity is altered in striatal medium-sized spiny neurons (MSNs) of transgenic mice expressing mHTT[9–13]. Because MSNs are the population that is affected first in Huntington's disease and NMDAR dysfunction can be detected at early disease stages, this alteration has long been thought to be a pathogenic trigger[14]. Notably, PACSIN1 promotes the endocytosis of NMDAR subtypes that contain GluN3A subunits. These subunits have been shown to prevent premature synapse plasticity and stabilization during early stages of postnatal brain development but are downregulated in adult brains[15,16]. In addition, the binding affinity of PACSIN1 for HTT depends on the length of

[1]Cellular Neurobiology and Neurophysiology Laboratories, Centro de Investigación Médica Aplicada (CIMA) y Universidad de Navarra, Pamplona, Spain. [2]Department of Cellular Biology, Immunology and Neuroscience, Medical School, Institut d'Investigacions Biomèdiques August Pi i Sunyer (IDIBAPS), University of Barcelona, Barcelona and Centro de Investigación Biomédica en Red sobre Enfermedades Neurodegenerativas (CIBERNED), Spain. [3]Institute of Medical Physiology, School of Medicine, University of Belgrade, Belgrade, Serbia. [4]Centre For Molecular Medicine and Therapeutics, Child and Family Research Institute, University of British Columbia, Vancouver, Canada. [5]Translational Laboratory in Genetic Medicine (TLGM), Department of Medicine, National University of Singapore and Agency for Science, Technology and Research (A*STAR), Singapore. [6]Departamento de Ciencias Médicas, Centro Regional de Investigaciones Biomédicas (CRIB), Facultad de Medicina, Universidad de Castilla-La Mancha, Albacete, Spain. [7]Center for Drug Discovery and Department of Neurobiology, Duke University Medical Center, Durham, North Carolina, USA. [8]Department of Anatomy, Hokkaido University School of Medicine, Sapporo, Japan. [9]Del E. Webb Center for Neuroscience, Aging and Stem Cell Research, Sanford-Burnham Medical Research Institute, La Jolla, California, USA. [10]Teva Pharmaceutical Industries Ltd, Petah Tikva, Israel. [11]Present address: Research Center on Aging, Department of Physiology and Biophysics, University of Sherbrooke, Sherbrooke, Quebec, Canada. [12]These authors contributed equally to this work. Correspondence should be addressed to I.P.-O. (otano@unav.es).

Received 6 March; accepted 20 May; published online 14 July 2013; doi:10.1038/nm.3246

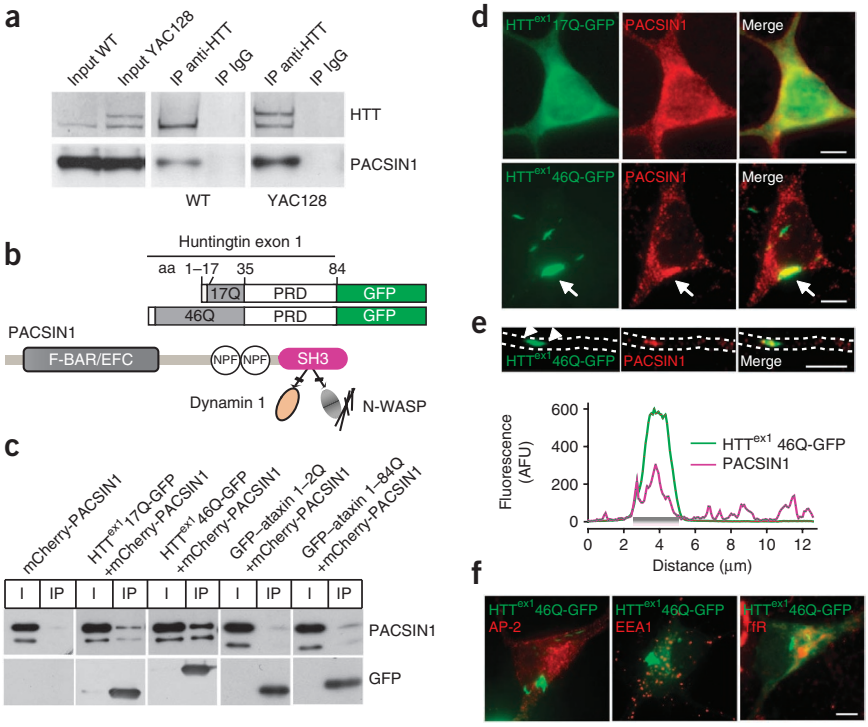

Figure 1 PACSIN1 binds to and colocalizes with mHTT. (**a**) Coimmunoprecipitation of HTT and PACSIN1 from striatal lysates of 3-month-old wild-type (WT) and YAC128 mice. HTT was immunoprecipitated with an antibody that recognizes both wild-type and mutant HTT. Immunoprecipitates (IP) were immunoblotted with the indicated antibodies. Additionally, 10% of the lysate (input) used for immunoprecipitation was loaded. (**b**) Scheme of the PACSIN1 structure indicating the F-BAR membrane deformation domain, the NPF (AsnProPhe) motifs responsible for GluN3A binding and the C-terminal SH3 domain. The SH3 domain mediates association with the proline-rich domain (PRD) of HTT but also links PACSIN1 to proteins of the endocytic machinery such as dynamin 1 and N-WASP. The location of GFP within the constructs used in this study is indicated. aa, amino acids. (**c**) Immunoblot using the indicated antibodies of lysates of HEK293 cells transfected with the indicated constructs and immunoprecipitated with a GFP-specific antibody. I, input lysates. (**d**) Representative images of striatal neurons transfected with HTT^{ex1}17Q-GFP or HTT^{ex1}46Q-GFP and stained for endogenous PACSIN1 48 h later. Arrows point to the localization of $mHTT^{ex1}$ and PACSIN1 in cytoplasmic aggregates. (**e**) Colocalization of $mHTT^{ex1}$ and PACSIN1 in dendritic aggregates as shown by line scan analysis of PACSIN1 and HTT^{ex1}46Q-GFP fluorescence (aggregate flanked by arrowheads in the images and shown by the gray bar in the graph). AFU, arbitrary fluorescence units. (**f**) Representative images of striatal neurons transfected with HTT^{ex1}46Q-GFP and immunostained for endogenous α-adaptin (AP-2), the early endosome marker EEA1 or transferrin receptor (TfR), which labels recycling endosomes. All scale bars, 5 μm.

the polyglutamine expansion[17], fulfilling a key criterion for pathogenic interactions[18], and PACSIN1 overexpression suppresses mHTT toxicity in *Drosophila* screens[4]. Thus we hypothesized that mHTT might interfere with the endocytic removal of GluN3A-containing NMDARs by PACSIN1, leading to age-inappropriate synapse destabilization during Huntington's disease pathogenesis.

We confirm that mHTT binds and sequesters PACSIN1 away from its normal cellular locations, causing the aberrant accumulation of juvenile GluN3A-containing NMDARs at the surface of striatal neurons. We also show that GluN3A expression is abnormally elevated across mouse models of Huntington's disease and in human Huntington's disease striatum, and that GluN3A overexpression in mice drives the degeneration of afferent synapses onto MSNs. Importantly, suppressing GluN3A reactivation corrected the early enhancement of NMDAR currents in MSNs from YAC128 mice, prevented both early stage and progressive dendritic spine pathology and ameliorated later motor and cognitive decline. Our results reveal a new mechanism that mediates NMDAR dysfunction and synapse loss in Huntington's disease—dysregulation of the expression of NMDARs that contain GluN3A subunits by altered endocytic trafficking—and identify a potential safe target for pharmacological therapy.

RESULTS

PACSIN1 binds to mHTT and is sequestered into aggregates

We began by verifying the interaction between HTT and PACSIN1 (refs. 4,17) with coimmunoprecipitation assays on striatal lysates from wild-type and YAC128 mice, which express full-length human *HTT* with 128 CAG repeats[19]. Although PACSIN1 interacted with both HTT variants, the interaction was stronger in the YAC128 striatum (2.23 ± 0.3-fold (mean ± s.e.m.) increase in PACSIN1 bound to HTT relative to wild type, $P = 0.005$; **Fig. 1a**). Coimmunoprecipitation assays from HEK293 cells cotransfected with PACSIN1 and GFP-tagged HTT exon 1 fragments spanning the proline-rich domain that binds PACSIN1 (ref. 17) and a normal or expanded polyglutamine tract (HTT^{ex1}17Q-GFP and HTT^{ex1}46Q-GFP, respectively) confirmed the polyglutamine dependence of the interaction and additionally showed that exon 1 is sufficient for PACSIN1 binding (**Fig. 1b**,**c**). We demonstrated specificity for HTT rather than the polyglutamine tract through experiments in which PACSIN1 did not interact with either normal or expanded ataxin 1, a polyglutamine repeat protein that is involved in spinocerebellar ataxia (**Fig. 1c**).

We next assessed whether binding to mHTT interferes with PACSIN1 localization or function in a cellular model of Huntington's disease[20]. We transfected cultured rat striatal neurons with HTT^{ex1} fragments and evaluated PACSIN1 localization by immunofluorescence. HTT^{ex1}46Q-GFP formed detectable intracellular aggregates in ~25% of neurons within 24–48 h, whereas HTT^{ex1}17Q-GFP showed diffuse expression (**Supplementary Fig. 1**). PACSIN1 immunostaining was punctate and distributed evenly in somatodendritic compartments of untransfected and HTT^{ex1}17Q-GFP–expressing neurons (**Fig. 1d**), but was enriched in somatodendritic HTT aggregates in neurons expressing HTT^{ex1}46Q-GFP (**Fig. 1d**,**e** and **Supplementary Fig. 1**). A quantitative colocalization analysis[21] yielded highly significant intensity correlation coefficient (ICQ) values for HTT^{ex1}46Q-GFP and PACSIN1 (0.26 ± 0.02 (mean ± s.e.m.), $P_{\text{sign test}} < 0.005$). We found lower ICQ values for HTT^{ex1}17Q-GFP (0.065 ± 0.01), which is consistent with weaker binding in biochemical assays. Other endocytic proteins were not enriched in aggregates (**Fig. 1f**), ruling out nonspecific sequestration.

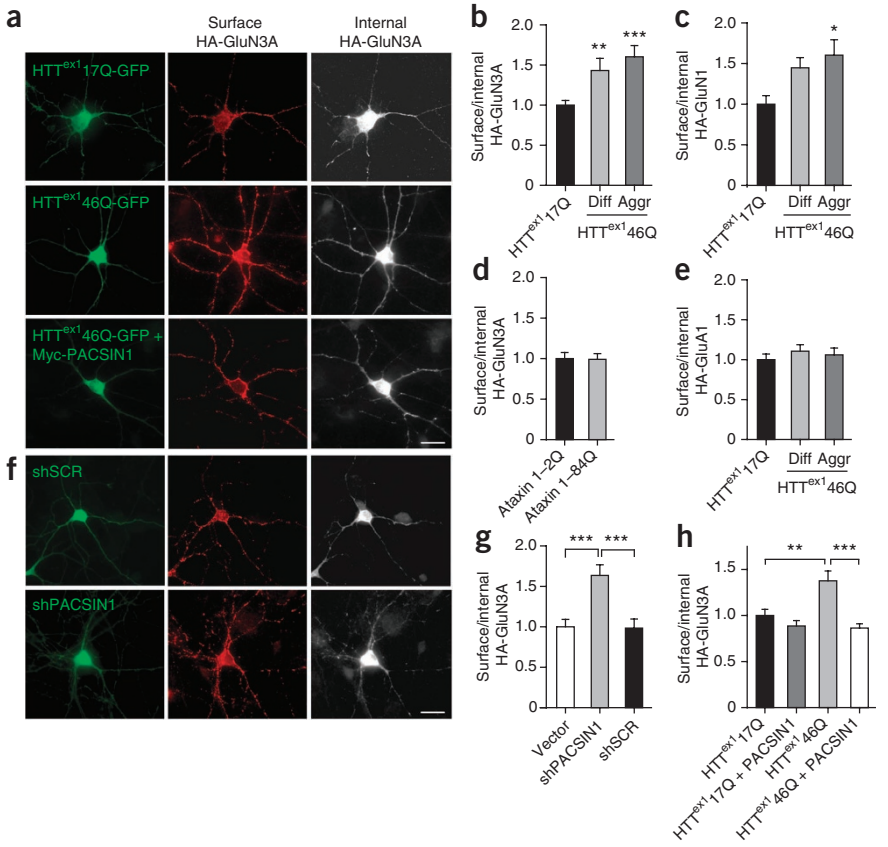

Figure 2 mHTT increases the surface expression of GluN3A-containing NMDARs. (**a**) Representative images of striatal neurons cotransfected with GFP-HTT^{ex1} and HA-GluN3A with or without Myc-PACSIN1. Surface (red) and internal receptors (white) were labeled with HA-specific antibody 48 h after transfection. Scale bar, 20 µm. (**b**–**e**) Quantification of the ratios of surface to internal GluN3A, GluN1 and GluA1 in neurons transfected with GFP-HTT^{ex1} or GFP–ataxin 1 (n = 20–54 neurons per condition from 2–3 independent experiments; $^{*}P < 0.05$, $^{**}P < 0.01$, $^{***}P < 0.001$ compared to HTT^{ex1}17Q-GFP, analysis of variance (ANOVA) followed by Bonferroni multiple comparison test). Diff, diffuse expression; aggr, aggregated expression. (**f**) Striatal neurons cotransfected with HA-GluN3A and PACSIN1-specific shRNA (shPACSIN1) or scrambled control shRNA (shSCR). Scale bar, 20 µm. (**g**) Quantification of the surface to internal ratios of HA-GluN3A in neurons transfected with shPACSIN1 (n = 17–52 neurons per condition from 2 independent experiments; $^{***}P < 0.001$, ANOVA followed by Bonferroni test). (**h**) Quantification of HA-GluN3A surface to internal ratios in HTT^{ex1}-GFP–transfected neurons after cotransfection with Myc-PACSIN1 (n = 51–69 neurons from 4 independent experiments; $^{**}P < 0.01$, $^{***}P < 0.001$, ANOVA followed by Bonferroni test). All data are shown as the mean ± s.e.m.

Redistribution into mHTT^{ex1} aggregates was associated with reductions of endogenous PACSIN1 amounts within their normal postsynaptic location, as quantified by decreases in dendrite-to-soma fluorescence intensity ratios and consistent with dendritic depletion of PACSIN1 in humans with Huntington's disease[17] (**Supplementary Fig. 2a**,**b**). The total amounts of PACSIN1 were unchanged (**Supplementary Fig. 2c**), indicating that reduced dendritic availability reflects altered subcellular distribution.

Increased surface GluN3A expression in neurons expressing mHTT

Because PACSIN1 controls the endocytic removal of GluN3A-containing NMDARs[8], stronger binding, subcellular sequestration or both by mHTT might be expected to interfere with ongoing endocytosis and affect plasma membrane expression. To test this idea, we cotransfected striatal neurons with hemagglutinin (HA)-tagged GluN3A and HTT^{ex1} variants and measured surface HA-GluN3A expression 48 h later using fluorescence-based antibody uptake assays. HTT^{ex1}46Q-GFP expression resulted in an accumulation of GluN3A at the neuronal surface (**Fig. 2a**,**b**) and concomitant increases in surface expression of the obligatory NMDAR subunit GluN1 (**Fig. 2c**), probably reflecting GluN1 assembly with GluN3A subunits which is required for their plasma-membrane transport and localization[22]. Notably, we observed increases in surface GluN3A expression in both neurons with diffuse HTT^{ex1}46Q-GFP expression and those with aggregated expression (**Fig. 2b**), suggesting that aggregation is not required and that binding to soluble mHTT species may be sufficient to alter PACSIN1 function. Supporting specificity for mHTT, polyglutamine expansions in ataxin 1 did not alter the surface expression of GluN3A (**Fig. 2d**). Because alterations in bulk endocytic recycling have been reported after mHTT expression in PC12 cells[23], we analyzed transferrin uptake but found no alterations in neurons transfected with HTT^{ex1}46Q-GFP by 48 h, a time when surface GluN3A levels were already elevated (**Supplementary Fig. 2d**,**e**). HTT^{ex1}46Q-GFP also did not affect the surface expression of the AMPA receptor subunit GluA1 (**Fig. 2e**), which is highly reliant on endocytic recycling[24]. These results indicate that GluN3A accumulation is not due to a general impairment in neuronal endocytosis.

Knockdown of PACSIN1 using a PACSIN1-specific shRNA (shPACSIN1; **Supplementary Fig. 3**) also increased surface GluN3A expression (**Fig. 2f**,**g**), demonstrating that PACSIN1 depletion can account for the mHTT-induced increase in surface GluN3A. We then asked whether an exogenous supply of PACSIN1 could counteract the effect of mHTT. Indeed, cotransfection of PACSIN1 rescued the surface accumulation of GluN3A subunits, which returned to control levels in HTT^{ex1}46Q-GFP–expressing neurons (**Fig. 2a**,**h**). These results show that loss of PACSIN1 function, probably due to mHTT binding, increases the surface expression of GluN3A-containing NMDARs in cultured striatal neurons.

Increased GluN3A in human Huntington's disease and mouse models

GluN3A protein is highly expressed in the brain during early postnatal and juvenile stages (postnatal day (P) 8–15 in mice and the first years of life in humans), but expression declines thereafter[25,26]. Quantitative immunoblot analysis showed that GluN3A undergoes a sharper downregulation in mouse striatum relative to other brain regions and is nearly absent by adulthood (**Supplementary Fig. 4**). In contrast, we found no developmental changes in GluN2B, which is the predominant NMDAR subunit type in striatum (**Supplementary Fig. 4**). These results support a physiological role for GluN3A downregulation in striatal NMDAR function and predict substantial effects of the disruption

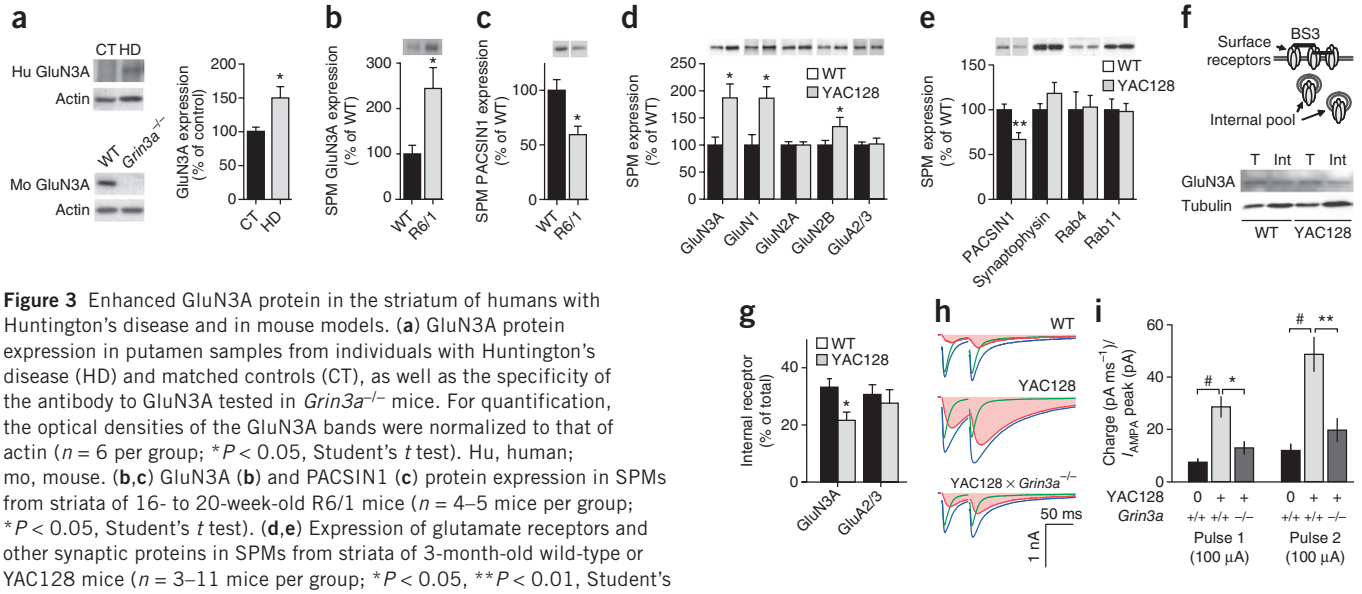

Figure 3 Enhanced GluN3A protein in the striatum of humans with Huntington's disease and in mouse models. (**a**) GluN3A protein expression in putamen samples from individuals with Huntington's disease (HD) and matched controls (CT), as well as the specificity of the antibody to GluN3A tested in *Grin3a*$^{-/-}$ mice. For quantification, the optical densities of the GluN3A bands were normalized to that of actin ($n = 6$ per group; $^{*}P < 0.05$, Student's t test). Hu, human; mo, mouse. (**b**,**c**) GluN3A (**b**) and PACSIN1 (**c**) protein expression in SPMs from striata of 16- to 20-week-old R6/1 mice ($n = 4$–5 mice per group; $^{*}P < 0.05$, Student's t test). (**d**,**e**) Expression of glutamate receptors and other synaptic proteins in SPMs from striata of 3-month-old wild-type or YAC128 mice ($n = 3$–11 mice per group; $^{*}P < 0.05$, $^{**}P < 0.01$, Student's t test). GluA2/3, GluA2 and GluA3. (**f**) Immunoblots showing GluN3A expression in striatal slices from 3-month-old YAC128 and wild-type mice that were either untreated (total, T) or incubated with BS3 (internal, Int). (**g**) Quantification of internal GluN3A and the GluA2/3 fraction ($n = 6$–8 mice per group; $^{*}P < 0.05$, Student's t test). (**h**) Excitatory postsynaptic currents (EPSCs) in MSNs after local afferent stimulation. Blue, compound NMDA and AMPAR responses; green, AMPAR components (50 µM AP5); red, NMDAR components obtained by subtraction. Traces are averages across all recordings ($n = 11$–15 cells or slices from 6–8 mice per genotype). (**i**) Quantification of the NMDAR component of the EPSCs integrated between 5 and 49 ms after stimulation divided by the peak of the AMPAR component ($^{\#}P < 0.005$, $^{*}P < 0.05$, $^{**}P < 0.01$, Kolmogorov-Smirnov test). All data are shown as the mean ± s.e.m.

of this downregulation. To evaluate whether GluN3A dysregulation occurs in humans, we analyzed postmortem brain tissue from controls and individuals with Huntington's disease. GluN3A protein expression in control human putamen, a subregion of the striatum, was low, but we detected a significant increase in GluN3A expression in affected individuals (**Fig. 3a** and **Supplementary Table 1**).

We next used the R6/1 and YAC128 mouse models of Huntington's disease to evaluate the timing of changes in GluN3A expression and their association with pathogenic events. R6/1 mice, which express N-terminally truncated human *HTT* carrying 115 CAG repeats[27], showed a progressive increase in striatal GluN3A expression relative to wild-type mice starting at around 12–16 weeks of age (**Supplementary Fig. 5a**). Because PACSIN1 is enriched at synapses where it mediates GluN3A removal[8,28], we biochemically isolated synaptic plasma membranes (SPMs) to determine whether increased GluN3A expression reflects increased residency at synaptic compartments associated with changes in PACSIN1 localization. Indeed, we detected a large increase in GluN3A expression (~2.5 fold) in SPMs from 20-week-old R6/1 mice, which matched a reduction in the synaptic abundance of PACSIN1 (**Fig. 3b**,**c**).

We obtained similar results in 3-month-old YAC128 mice (**Fig. 3d**,**e** and **Supplementary Fig. 5b**). Increased GluN3A expression in striatal SPMs was paralleled by increases in GluN1 and GluN2B, suggesting that GluN3A forms heteromultimeric NMDAR complexes that include these subunits (**Fig. 3d**), and was associated with reduced synaptic PACSIN1 expression (**Fig. 3e**). We did not detect changes in GluN2A, GluA2 or GluA3, in presynaptic proteins such as synaptophysin or in the trafficking regulators Rab4 or Rab11 (**Fig. 3d**,**e**). Further fractionation of striatal synaptic membranes showed increased GluN3A expression in both detergent-soluble (non–postsynaptic density (PSD)) and insoluble (PSD) fractions, which is consistent with the subsynaptic localization pattern that is characteristic of GluN3A[8] (**Supplementary Fig. 6**). Overall PACSIN1 protein expression was unchanged (93% ± 3% (mean ± s.e.m.) of wild type, $P = 0.19$), corroborating our culture data and further indicating that lower synaptic expression of PACSIN1 reflects subcellular redistribution. At this early disease stage, GluN3A expression was not altered in brain regions that are affected later in the progression of Huntington's disease, such as the cortex and hippocampus (**Supplementary Fig. 5b**). Immunolabeling further showed that increases in GluN3A expression occurred mainly in DARPP-32–labeled MSNs (**Supplementary Fig. 5c**,**d**).

To test whether elevated GluN3A expression reflects a defect in endocytosis, as would be predicted if subcellular sequestration of PACSIN1 by mHTT is the underlying mechanism, we incubated striatal slices from control and YAC128 mice with the membrane-impermeable cross-linker bissulfosuccinimidyl suberate (BS3). This reagent cross-links surface receptors to form high-molecular-weight complexes that can be separated from unlinked intracellular receptors by electrophoresis, allowing a quantification of the internal receptor pool (**Fig. 3f**). These experiments revealed a significantly reduced fraction of intracellular GluN3A in YAC128 striatum but no changes in GluA2 or GluA3 (**Fig. 3f**,**g**). We additionally looked for contributions of altered transcription but found no significant changes in GluN3A mRNA levels in either R6/1 or YAC128 striatum at times when the synaptic and surface expression of GluN3A protein was increased by approximately two-fold (**Supplementary Fig. 5e**). These results confirm that GluN3A is redistributed to the plasma membrane and synaptic compartments in mouse models of Huntington's disease. They further show that striatal GluN3A dysregulation begins before or around the onset of motor or cognitive symptoms[29–32], long preceding neuronal loss, and may thus be an early disease mechanism in Huntington's disease pathophysiology. We also observed increases in GluN3A

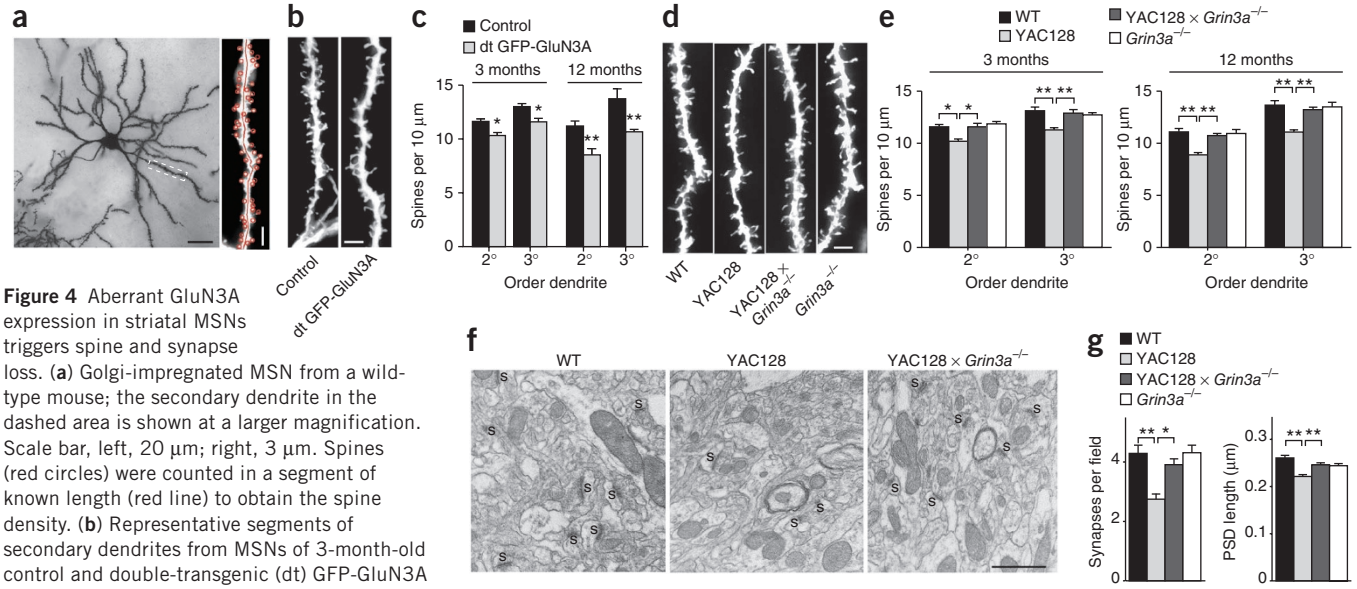

Figure 4 Aberrant GluN3A expression in striatal MSNs triggers spine and synapse loss. (**a**) Golgi-impregnated MSN from a wild-type mouse; the secondary dendrite in the dashed area is shown at a larger magnification. Scale bar, left, 20 µm; right, 3 µm. Spines (red circles) were counted in a segment of known length (red line) to obtain the spine density. (**b**) Representative segments of secondary dendrites from MSNs of 3-month-old control and double-transgenic (dt) GFP-GluN3A mice. Scale bar, 3 µm. (**c**) Quantification of spine densities in dt GFP-GluN3A mice and age-matched controls (n = 12–18 neurons from 4 mice per genotype; $^*P < 0.01$, $^{**}P < 0.001$ compared to wild type, Student's t test). (**d**) Dendritic segments from MSNs of 3-month-old wild-type, YAC128, YAC128 × *Grin3a*$^{-/-}$ and *Grin3a*$^{-/-}$ mice. Scale bar, 3 µm. (**e**) Quantification of spine densities in MSNs from mice of the indicated ages and genotypes (n = 24–32 neurons from 6–8 mice per group; $^*P < 0.01$, $^{**}P < 0.001$, ANOVA followed by Bonferroni multiple comparison test). (**f**,**g**) Electron microscopy analysis of the number and size of excitatory synapses in striatum of 3-month-old mice. Scale bar, 1 µm (n = 3 mice per genotype; $^*P < 0.01$, $^{**}P < 0.001$, Kruskal-Wallis test followed by Bonferroni multiple comparison test). All data are shown as the mean ± s.e.m.

expression preceding symptom onset in a third Huntington's disease model, *Hdh*^{Q111} (where *Hdh* is the murine gene homolog of *HTT*) knock-in mice, in which the phenotype is much delayed[33] (**Supplementary Fig. 5f**).

Suppressing GluN3A corrects NMDAR dysfunction in YAC128 mice

Alterations in NMDAR function have been reported in MSNs of YAC128 mice by 1 month of age. These defects involve long-lasting responses to glutamate release and have been attributed to increased activation of extrasynaptic NMDARs[13]. Because a distinguishing feature of GluN3A-containing receptors is their perisynaptic and extrasynaptic localization[8,34], and GluN3A expression was increased early in synaptosomal subfractions from YAC128 striatum that are enriched in extrasynaptic plasma membrane receptors (non-PSD), we asked whether the electrophysiological defect could be explained by elevated GluN3A expression.

We crossed YAC128 mice with *Grin3a*$^{-/-}$ (*Grin3a* is the gene encoding GluN3A) mice and compared NMDAR responses after intense paired-pulse afferent stimulation in wild-type, YAC128 and YAC128 mice lacking GluN3A[13]. We obtained isolated NMDAR responses by calculating the difference between the responses recorded in the absence and presence of the NMDAR blocker (2*R*)-amino-5-phosphonovaleric acid (AP5). We detected no changes in the AMPAR-mediated component obtained in AP5 but found large differences in the decay kinetics of the isolated NMDAR component ($P < 0.005$ for YAC128 compared to wild type; **Fig. 3h**,**i**), confirming previous observations[13]. These differences were largely abolished in YAC128 mice lacking GluN3A (**Fig. 3h**,**i**), indicating that GluN3A is required for the mHTT-induced enhancement in NMDAR currents and consistent with the possibility that aberrant GluN3A expression underlies the earliest events of Huntington's disease pathophysiology.

Suppressing GluN3A rescues synapse pathology in YAC128 mice

Dendritic dystrophy and loss of glutamatergic spiny synapses are early degenerative changes in Huntington's disease[7,35,36] that might underlie symptom onset. Because enhancement of GluN3A function in the hippocampus drives synapse elimination[16], we asked whether aberrant GluN3A expression could contribute to the synaptic pathology. We first used Golgi impregnation techniques to measure dendritic spines, which are sites where excitatory synapses form, in YAC128 mice at times when GluN3A expression was elevated (**Fig. 4a**). Spine numbers were decreased in dendrites of YAC128 MSNs by 3 months of age (12–15% decrease compared to wild type), and this decay worsened with age (**Supplementary Fig. 7**).

To test whether abnormal accumulation of GluN3A in adult MSNs could explain the progressive spine loss induced by mHTT, we measured spine densities in transgenic mice that overexpress GluN3A into adulthood (double-transgenic GFP-GluN3A mice). These mice were generated by crossing mice expressing GFP-tagged GluN3A under the control of the *tetO* promoter with mice expressing the tetracycline-controlled transactivator (tTA) under the *Camk2a* promoter[16]; the *Camk2a* promoter drives transgene expression into MSNs[34]. MSNs from double-transgenic GFP-GluN3A mice showed a pattern of spine loss that was remarkably similar to that observed in YAC128 mice (~11% decrease in double-transgenic mice relative to control littermates by 3 months of age, with larger spine losses at later stages; **Fig. 4b**,**c**, compare with **Supplementary Fig. 7**).

We then reasoned that if the spine loss in MSNs was caused by enhanced GluN3A function, it should be prevented by lowering GluN3A expression. To test this idea, we re-examined spine densities in wild-type and YAC128 mice in the presence and absence of GluN3A. Lack of GluN3A prevented both the early reductions in spine numbers in YAC128 mice and the progressive synaptic disconnection detected as a larger loss of MSN spines

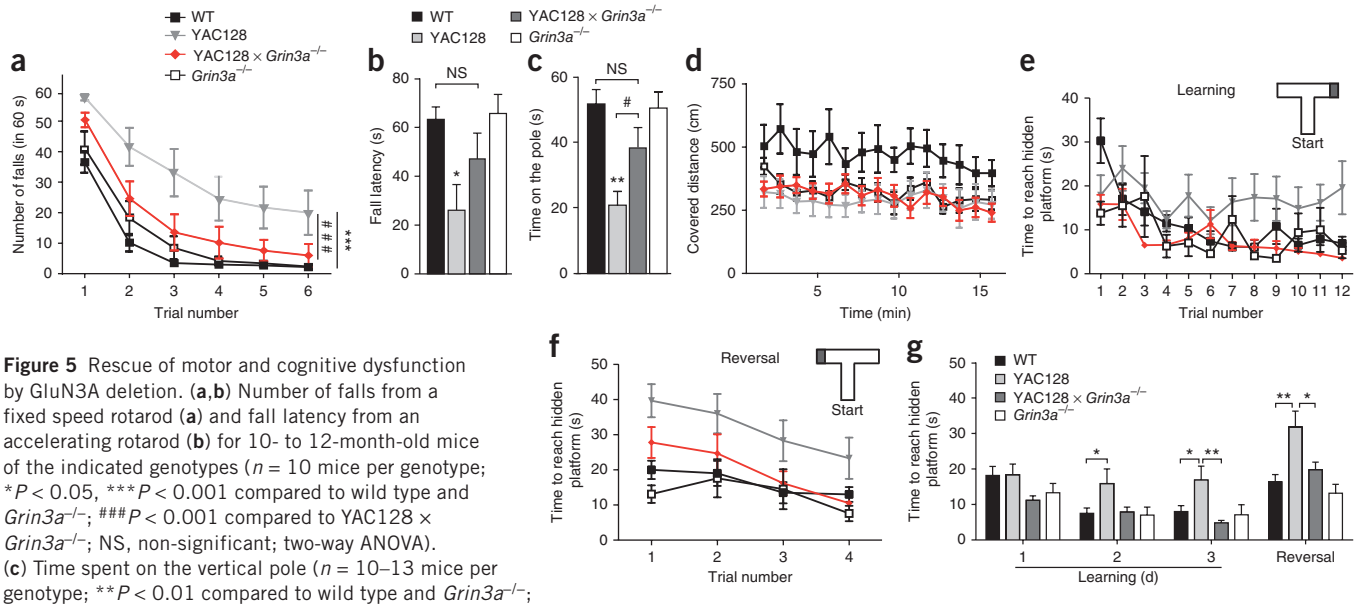

Figure 5 Rescue of motor and cognitive dysfunction by GluN3A deletion. (**a**,**b**) Number of falls from a fixed speed rotarod (**a**) and fall latency from an accelerating rotarod (**b**) for 10- to 12-month-old mice of the indicated genotypes ($n = 10$ mice per genotype; $^{*}P < 0.05$, $^{***}P < 0.001$ compared to wild type and *Grin3a*$^{-/-}$; $^{\#\#\#}P < 0.001$ compared to YAC128 × *Grin3a*$^{-/-}$; NS, non-significant; two-way ANOVA). (**c**) Time spent on the vertical pole ($n = 10$–13 mice per genotype; $^{**}P < 0.01$ compared to wild type and *Grin3a*$^{-/-}$; $^{\#}P < 0.05$ compared to YAC128 × *Grin3a*$^{-/-}$; one-way ANOVA followed by Tukey's test). (**d**) Spontaneous locomotor activity in the open-field test. ($n = 10$ mice per genotype). (**e**,**f**) Times to reach the hidden platform in the swimming T maze during the training phase (3 d, four trials per day; **e**) and after platform reversal on day 4 (**f**). (**g**) Daily averages of the times to reach a hidden platform ($n = 5$–11 mice per genotype; $^{*}P < 0.05$, $^{**}P < 0.01$, one-way ANOVA followed by Tukey's test). All data are shown as the mean ± s.e.m.

at later stages of disease (**Fig. 4d**,**e**). In contrast, spine densities were not altered in MSNs from adult *Grin3a*$^{-/-}$ mice (**Fig. 4d**,**e**), indicating that blocking GluN3A expression targets the synaptic pathology in Huntington's disease without affecting basal spine numbers in controls. This result differs from the increased spine density reported in *Grin3a*$^{-/-}$ cortical neurons[15] and probably reflects the lower GluN3A expression retained in adult striatum (**Supplementary Fig. 4**).

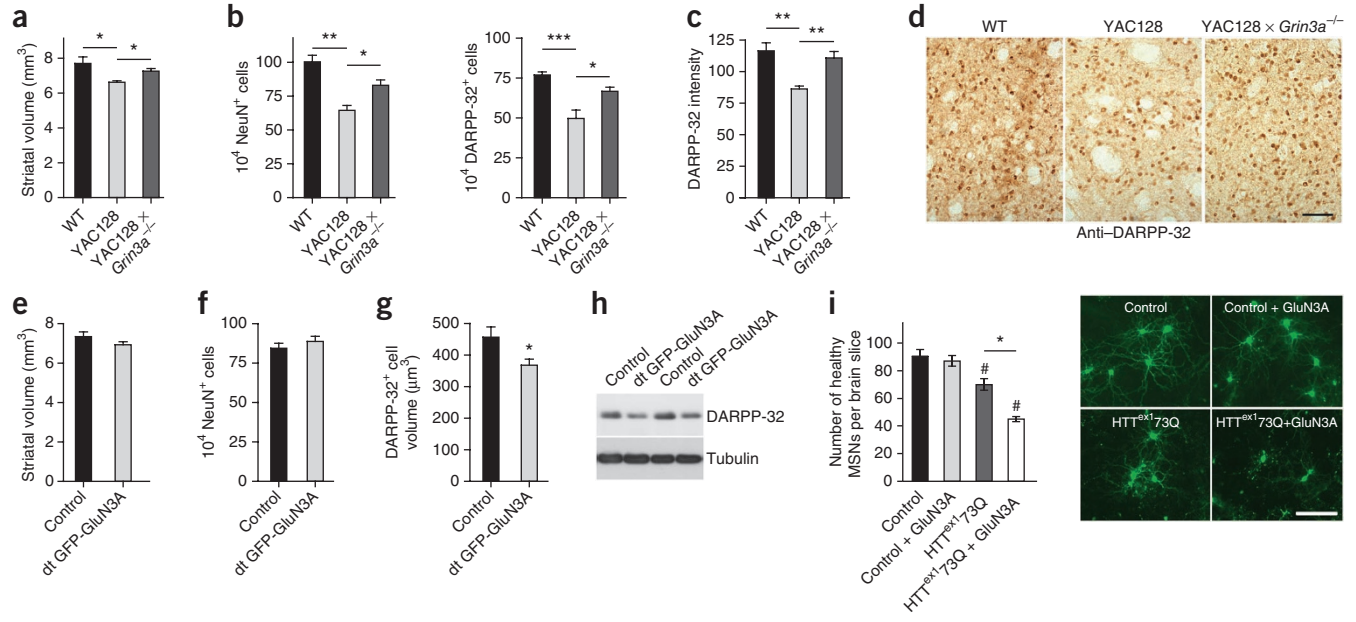

Figure 6 Suppressing GluN3A prevents, and increasing GluN3A potentiates, mHTT-induced death of striatal MSNs. (**a**,**b**) Stereological measurements of striatal volume and number of NeuN-positive and DARPP-32–positive neurons in 16-month-old wild-type, YAC128 and YAC128 × *Grin3a*$^{-/-}$ mice ($n = 6$ mice per genotype; $^{*}P < 0.05$, $^{**}P < 0.01$, $^{***}P < 0.001$, one-way ANOVA followed by Tukey's test). (**c**) DARPP-32 staining intensity per cell measured in surviving MSNs ($n = 6$ mice per genotype; $^{**}P < 0.01$, one-way ANOVA followed by Tukey's test). (**d**) Representative microphotographs of DARPP-32–stained striata. Scale bar, 70 μm. (**e**,**f**) Stereological measurements of striatal volume and number of NeuN-positive neurons in 16-month-old control and dt GFP-GluN3A mice ($n = 9$ mice per genotype). (**g**) Measurements of cell volume in DARPP-32–positive neurons ($n = 9$ mice per genotype; $^{*}P < 0.05$, Student's *t* test). (**h**) Representative immunoblots showing striatal DARPP-32 protein expression in 24-month-old control and dt GFP-GluN3A mice. (**i**) Left, the number of nondegenerating MSNs per brain slice assessed by coexpression of YFP with the indicated constructs ($n = 15$–18 slices scored per condition; $^{*}P < 0.01$, $^{\#}P < 0.01$ relative to control slices, ANOVA followed by Tukey's test; data are representative of 3 independent experiments). Right, representative images of striatal slices in the YFP channel. Scale bar, 100 μm. All data are shown as the mean ± s.e.m.

At high resolution, electron microscopy revealed a marked loss of asymmetric glutamatergic synapses onto MSNs of YAC128 mice, which was rescued by GluN3A deletion (**Fig. 4f**,**g**). In addition, postsynaptic densities were smaller in YAC128 mice (**Fig. 4g**), which is consistent with earlier studies in which GluN3A overexpression decreased synapse size[16], and this deficit was also rescued by suppressing GluN3A (**Fig. 4g**). These results show that diminished synaptic connectivity in MSNs from YAC128 mice begins at early stages, matching the timing of GluN3A dysregulation, and can be rescued by deleting GluN3A or replicated by transgenically overexpressing GluN3A.

Suppressing GluN3A ameliorates motor and cognitive dysfunction

We next assessed the impact of GluN3A on Huntington's disease–like symptoms using striatum-dependent motor and cognitive tasks. YAC128 mice showed impaired motor learning by 10 months of age, as indicated by increased failures when learning a fixed-speed rotarod task, and impaired coordination, as indicated by a shorter latency to fall from an accelerating rotarod. Both deficits were improved in YAC128 mice lacking GluN3A (**Fig. 5a**,**b**). A vertical pole test, another measure of motor coordination, showed that YAC128 mice spent less time on the pole than wild-type mice, an effect that was again rescued by GluN3A deletion (**Fig. 5c**). Nevertheless, the hypokinetic phenotype shown by YAC128 mice in an open field was still apparent in YAC128 mice lacking GluN3A (**Fig. 5d**). Neither weight gain nor loss of muscle tone was rescued by GluN3A deletion (**Supplementary Fig. 8**), ruling out the possibility that improvements in coordination resulted from reversal of these parameters.

We evaluated cognitive function using a swimming T-maze task[37] (**Fig. 5e**–**g**). YAC128 mice showed a pronounced impairment during the learning phase, whereas YAC128 mice lacking GluN3A performed as well as wild-type mice (**Fig. 5e**,**g**). On day 4, we switched the platform to the opposite arm of the T maze to probe reversal (strategy-shifting) learning. YAC128 mice required longer than wild-type mice to reach the new platform location in all trials, and this defect was rescued by GluN3A deletion (**Fig. 5f**,**g**).

Suppressing GluN3A rescues mHTT toxicity

To investigate whether abnormally increased GluN3A expression contributes to later striatal atrophy and MSN degeneration, we performed stereological analyses in 16-month-old mice, an age at which neuronal death can be reproducibly detected in the YAC128 model[19]. Suppressing GluN3A expression in YAC128 mice rescued striatal atrophy and reductions in NeuN-positive and DARPP-32–positive neurons and normalized DARPP-32 expression in surviving MSNs (**Fig. 6a**–**d**); DARPP-32 is a key component of MSN dopamine signaling cascades that is downregulated in Huntington's disease mouse models from early stages[38].

Analogous analyses in control and double-transgenic GFP-GluN3A mice showed that GluN3A overexpression does not cause striatal atrophy or neuronal loss *per se* by 16 months of age (**Fig. 6e**,**f**) but mimics other neuropathological features of Huntington's disease, including reductions in the size of MSNs[39] (**Fig. 6g**) and striatal DARPP-32 expression[40] (100 ± 16 (mean ± s.e.m., integrated density values) in control mice compared to 61 ± 5 in double-transgenic GFP-GluN3A mice; $n = 6$; $P < 0.05$; **Fig. 6h**). We next conducted experiments in a rat corticostriatal slice model[41] to test whether increased GluN3A expression influences the susceptibility of MSNs to mHTT toxicity. We cotransfected slice explants with expanded HTT^{ex1} (HTT^{ex1}73Q-GFP) along with GluN3A and assessed MSN degeneration by coexpression of yellow fluorescent protein (YFP). The number of surviving MSNs was decreased in brain slices cotransfected with mHTT and GluN3A relative to slices transfected with mHTT alone (**Fig. 6i**). Thus, increased GluN3A expression recapitulates features of Huntington's disease neuronal dysfunction, such as MSN shrinkage and disturbed signaling, and renders MSNs more vulnerable to mHTT toxicity.

DISCUSSION

We identify a new early stage disease mechanism that underlies NMDAR dysfunction and synapse loss in Huntington's disease: subcellular sequestration of the endocytic adaptor PACSIN1 by mHTT leaves an overabundance of NMDARs containing GluN3A subunits in the plasma membrane and at postsynaptic sites of striatal neurons. The new mechanism provides a missing link between two major phenomena previously known to be impaired by HTT mutations, defects in protein trafficking and impaired NMDAR transmission. GluN3A dysregulation targeted MSNs, the vulnerable population in Huntington's disease striatum, and was an early feature across Huntington's disease mouse models. Knocking out GluN3A in Huntington's disease mice corrected a full sequence of early-to-late pathophysiological events, demonstrating a crucial role for GluN3A in disease pathogenesis *in vivo*: it normalized NMDAR currents; fully prevented synapse degeneration; rescued motor and cognitive decline; and reduced striatal cell death.

Our data extend previous findings pointing toward GluN3A subunits as a synapse destabilizing or pruning factor[16] and show the pathogenic effects of aberrant reactivation in the adult brain of a pruning mechanism that is normally restricted to developmental stages. In the normal brain, PACSIN1-mediated retrieval of GluN3A from synapses contributes to receptor downregulation and is thought to provide a crucial signal for synaptic plasticity and growth and for robust information storage by allowing the replacement of immature with mature NMDAR subtypes[8,16]. Factors that inhibit PACSIN1 function, such as dominant-negative variants of PACSIN1 (ref. 8) or mHTT, increase surface and synaptic GluN3A expression, yielding a higher proportion of small, immature synapses. Although the precise mechanisms by which mHTT alters PACSIN1 distribution remain unclear, our observations of reduced synaptic PACSIN1 expression in young YAC128 mice, months before aggregates are present[42], and surface accumulation of GluN3A in striatal neurons with no detectable HTT aggregates argue against a requirement for aggregation. This fits with current concepts linking soluble mHTT species, rather than aggregates, to cytotoxicity[20,43,44]. But PACSIN1 redistribution into microaggregates not visible by light microscopy cannot be ruled out, and the question of whether PACSIN1 binds to particular conformations of mHTT remains open.

Regarding the stoichiometry of GluN3A-containing NMDARs in Huntington's disease striatum, our biochemical fractionation results indicate the presence of GluN1 and GluN2B subunits. This is consistent with biochemical evidence for assembly of GluN3A and GluN2B subunits in striatal tissue[34] and reports attributing the enhanced NMDAR responses in YAC128 mice to GluN2B-containing NMDARs[13,45], as well as our finding that suppressing GluN3A corrects the alteration. GluN3A-containing subtypes are less anchored to PSDs than conventional NMDARs (GluN1-GluN2 heteromers), and GluN3A overexpression has been shown to impair the postsynaptic stabilization of GluN2B-containing NMDARs[34], which might facilitate their diffusion toward extrasynaptic sites, providing a testable cell-biological mechanism for the increased extrasynaptic GluN2B-mediated currents in YAC models[13]. Along with synapse loss and

enhanced extrasynaptic NMDARs, elevated GluN3A expression could explain features of altered glutamatergic transmission that have been observed in presymptomatic Huntington's disease mice and cannot be accounted for by the increased GluN2B-mediated currents without considering the presence of additional subunits in the receptor complex. These include anomalously reduced long-term potentiation[46–48] and decreased magnesium sensitivity of NMDAR currents[11,49], both of which have been reported in GluN3A-overexpressing mice[16].

An imbalance between synaptic and extrasynaptic NMDAR activity is thought to be crucial for neurodegeneration because the two receptor populations signal to cell-survival and death pathways, respectively[50], and increased extrasynaptic activity has been linked to cell death in Huntington's disease[13,43]. Enhanced GluN3A expression could contribute to cell death by driving or aggravating this imbalance in two ways. First, it might trigger the activation of death pathways by increasing extrasynaptic NMDAR localization. Second, MSNs receive dense glutamatergic input from cortical axons, and the synaptic disconnection driven by GluN3A could inhibit prosurvival signaling pathways coupled to synaptic NMDAR activation[50,51]. But GluN3A-containing subtypes flux less Ca^{2+} than other NMDAR subtypes[22], and data from our own laboratory support a neuroprotective action of GluN3A overexpression in acute excitotoxic cell-death assays[34,52], which might explain the paradoxical resistance to acute excitotoxic insults observed in Huntington's disease models[53,54]. Nonetheless, aberrant GluN3A expression over the much longer time course relevant to Huntington's disease (that is, decades rather than minutes) could have deleterious effects due to inhibition of synaptotrophic NMDAR activity and/or chronically disturbed signaling by extrasynaptic NMDARs activated by ambient glutamate.

In summary, we uncover a role for GluN3A dysregulation in Huntington's disease and provide a rationale for the use of therapies targeting GluN3A or PACSIN1 early in the course of the disease to ameliorate cognitive or motor problems, halt disease progression or both. An advantage of targeting GluN3A (as compared to other NMDAR subunits) is that it is lacking in adult brains for the most part and would allow for the selective blocking of a pathological trait without hampering normal synaptic function.

METHODS

Methods and any associated references are available in the online version of the paper.

Note: Supplementary information is available in the online version of the paper.

ACKNOWLEDGMENTS

We thank S. Finkbeiner (Gladstone Institute, University of California San Francisco), H. Zoghbi (Baylor College of Medicine), T. Yamamoto (University of Tokyo) and M. Ehlers (Pfizer Neuroscience) for providing reagents, A. Zandueta, C. Rodríguez-Viña, F. Ballesteros, X. Remírez and M. Montañana for excellent technical help, M. Galarraga for advice with image analysis, and M. Ehlers, M. Arrasate, T. Aragón, J.A. Esteban and B.D. Philpot for critical readings of the manuscript. This work was funded by the Unión Temporal de Empresas (UTE) project at the Centro de Investigación Médica Aplicada, Gobierno de Navarra, and Spanish Ministry of Science grants (SAF2010-20636 and CSD2008-00005 to I.P.-O., BFU2009-12160 to J.F.W. and SAF2011-29507 to J.A.), grants from the Hereditary Disease Foundation (to I.P.-O. and D.C.L.), US National Institutes of Health grants P01 HD29587, P01 ES016738 and R01 EY05477 (to S.A.L.) and grants from the Cure Huntington's Disease Initiative and the Canadian Institutes of Health Research (to M.R.H.). M.R.H., a Killam University Professor, holds a Canada Research Chair in Human Genetics.

AUTHOR CONTRIBUTIONS

S.M. performed and analyzed the biochemical experiments in cultured neurons, recombinant cells and YAC128 mice, the imaging experiments in cultured neurons and the spine morphology measurements and collaborated with A.G. on neuropathological studies. A.G. performed and analyzed biochemical experiments in humans and R6/1 and knock-in mice and the behavioral experiments. M.M.P. performed electrophysiological recordings. M.A.P. performed and analyzed behavioral experiments. R.M.-T. contributed to mouse genotyping and conducted biochemical fractionation and real-time PCR assays. J.M.-H. and R.L. performed and analyzed electron microscopy studies. L.S.K. and D.C.L. performed and analyzed slice culture experiments. J.T.-P. performed the initial biochemical experiments in R6/1 mice. M.R.H. and R.K.G. provided the YAC128 mice. N.N. and S.A.L. provided the *Grin3a*$^{-/-}$ mice. M.W. made the GluN3A-specific antibody used in biochemical and immunocytochemical analyses. J.A. designed and supervised experiments. J.F.W. designed and analyzed electrophysiological and fluorescence colocalization experiments and contributed to the manuscript writing. I.P.-O. conceived the study, designed experiments, analyzed data and wrote the paper.

COMPETING FINANCIAL INTERESTS

The authors declare no competing financial interests.

1. DiFiglia, M. *et al.* Aggregation of huntingtin in neuronal intranuclear inclusions and dystrophic neurites in brain. *Science* **277**, 1990–1993 (1997).
2. DiFiglia, M. *et al.* Huntingtin is a cytoplasmic protein associated with vesicles in human and rat brain neurons. *Neuron* **14**, 1075–1081 (1995).
3. Schaffar, G. *et al.* Cellular toxicity of polyglutamine expansion proteins: mechanism of transcription factor deactivation. *Mol. Cell* **15**, 95–105 (2004).
4. Kaltenbach, L.S. *et al.* Huntingtin interacting proteins are genetic modifiers of neurodegeneration. *PLoS Genet.* **3**, e82 (2007).
5. Goehler, H. *et al.* A protein interaction network links GIT1, an enhancer of huntingtin aggregation, to Huntington's disease. *Mol. Cell* **15**, 853–865 (2004).
6. Qin, Z.H. *et al.* Huntingtin bodies sequester vesicle-associated proteins by a polyproline-dependent interaction. *J. Neurosci.* **24**, 269–281 (2004).
7. Li, J.Y., Plomann, M. & Brundin, P. Huntington's disease: a synaptopathy? *Trends Mol. Med.* **9**, 414–420 (2003).
8. Pérez-Otaño, I. *et al.* Endocytosis and synaptic removal of NR3A-containing NMDA receptors by PACSIN1/syndapin1. *Nat. Neurosci.* **9**, 611–621 (2006).
9. Levine, M.S. *et al.* Enhanced sensitivity to *N*-methyl-d-aspartate receptor activation in transgenic and knock-in mouse models of Huntington's disease. *J. Neurosci. Res.* **58**, 515–532 (1999).
10. Zeron, M.M. *et al.* Increased sensitivity to *N*-methyl-d-aspartate receptor-mediated excitotoxicity in a mouse model of Huntington's disease. *Neuron* **33**, 849–860 (2002).
11. Cepeda, C. *et al.* NMDA receptor function in mouse models of Huntington disease. *J. Neurosci. Res.* **66**, 525–539 (2001).
12. Laforet, G.A. *et al.* Changes in cortical and striatal neurons predict behavioral and electrophysiological abnormalities in a transgenic murine model of Huntington's disease. *J. Neurosci.* **21**, 9112–9123 (2001).
13. Milnerwood, A.J. *et al.* Early increase in extrasynaptic NMDA receptor signaling and expression contributes to phenotype onset in Huntington's disease mice. *Neuron* **65**, 178–190 (2010).
14. Beal, M.F. *et al.* Replication of the neurochemical characteristics of Huntington's disease by quinolinic acid. *Nature* **321**, 168–171 (1986).
15. Das, S. *et al.* Increased NMDA current and spine density in mice lacking the NMDA receptor subunit NR3A. *Nature* **393**, 377–381 (1998).
16. Roberts, A.C. *et al.* Downregulation of NR3A-containing NMDARs is required for synapse maturation and memory consolidation. *Neuron* **63**, 342–356 (2009).
17. Modregger, J., DiProspero, N.A., Charles, V., Tagle, D.A. & Plomann, M. PACSIN 1 interacts with huntingtin and is absent from synaptic varicosities in presymptomatic Huntington's disease brains. *Hum. Mol. Genet.* **11**, 2547–2558 (2002).
18. Lim, J. *et al.* Opposing effects of polyglutamine expansion on native protein complexes contribute to SCA1. *Nature* **452**, 713–718 (2008).
19. Slow, E.J. *et al.* Selective striatal neuronal loss in a YAC128 mouse model of Huntington disease. *Hum. Mol. Genet.* **12**, 1555–1567 (2003).
20. Arrasate, M., Mitra, S., Schweitzer, E.S., Segal, M.R. & Finkbeiner, S. Inclusion body formation reduces levels of mutant huntingtin and the risk of neuronal death. *Nature* **431**, 805–810 (2004).
21. Li, Q. *et al.* A syntaxin 1, Gα(o), and N-type calcium channel complex at a presynaptic nerve terminal: analysis by quantitative immunocolocalization. *J. Neurosci.* **24**, 4070–4081 (2004).
22. Perez-Otaño, I. *et al.* Assembly with the NR1 subunit is required for surface expression of NR3A-containing NMDA receptors. *J. Neurosci.* **21**, 1228–1237 (2001).
23. Li, X. *et al.* Mutant huntingtin impairs vesicle formation from recycling endosomes by interfering with Rab11 activity. *Mol. Cell Biol.* **29**, 6106–6116 (2009).
24. Park, M., Penick, E.C., Edwards, J.G., Kauer, J.A. & Ehlers, M.D. Recycling endosomes supply AMPA receptors for LTP. *Science* **305**, 1972–1975 (2004).

25. Wong, H.K. *et al.* Temporal and regional expression of NMDA receptor subunit NR3A in the mammalian brain. *J. Comp. Neurol.* **450**, 303–317 (2002).
26. Henson, M.A., Roberts, A.C., Perez-Otaño, I. & Philpot, B.D. Influence of the NR3A subunit on NMDA receptor functions. *Prog. Neurobiol.* **91**, 23–37 (2010).
27. Mangiarini, L. *et al.* Exon 1 of the HD gene with an expanded CAG repeat is sufficient to cause a progressive neurological phenotype in transgenic mice. *Cell* **87**, 493–506 (1996).
28. Qualmann, B., Roos, J., DiGregorio, P.J. & Kelly, R.B. Syndapin I, a synaptic dynamin-binding protein that associates with the neural Wiskott-Aldrich syndrome protein. *Mol. Biol. Cell* **10**, 501–513 (1999).
29. Canals, J.M. *et al.* Brain-derived neurotrophic factor regulates the onset and severity of motor dysfunction associated with enkephalinergic neuronal degeneration in Huntington's disease. *J. Neurosci.* **24**, 7727–7739 (2004).
30. Mazarakis, N.K. *et al.* Deficits in experience-dependent cortical plasticity and sensory-discrimination learning in presymptomatic Huntington's disease mice. *J. Neurosci.* **25**, 3059–3066 (2005).
31. Van Raamsdonk, J.M. *et al.* Phenotypic abnormalities in the YAC128 mouse model of Huntington disease are penetrant on multiple genetic backgrounds and modulated by strain. *Neurobiol. Dis.* **26**, 189–200 (2007).
32. Graham, R.K. *et al.* Levels of mutant huntingtin influence the phenotypic severity of Huntington disease in YAC128 mouse models. *Neurobiol. Dis.* **21**, 444–455 (2006).
33. Wheeler, V.C. *et al.* Early phenotypes that presage late-onset neurodegenerative disease allow testing of modifiers in Hdh CAG knock-in mice. *Hum. Mol. Genet.* **11**, 633–640 (2002).
34. Martínez-Turrillas, R. *et al.* The NMDA receptor subunit GluN3A protects against 3-nitroproprionic–induced striatal lesions via inhibition of calpain activation. *Neurobiol. Dis.* **48**, 290–298 (2012).
35. Graveland, G.A., Williams, R.S. & DiFiglia, M. Evidence for degenerative and regenerative changes in neostriatal spiny neurons in Huntington's disease. *Science* **227**, 770–773 (1985).
36. Cummings, D.M., Cepeda, C. & Levine, M.S. Alterations in striatal synaptic transmission are consistent across genetic mouse models of Huntington's disease. *ASN Neuro* **2**, e00036 (2010).
37. Van Raamsdonk, J.M. *et al.* Cognitive dysfunction precedes neuropathology and motor abnormalities in the YAC128 mouse model of Huntington's disease. *J. Neurosci.* **25**, 4169–4180 (2005).
38. Bibb, J.A. *et al.* Severe deficiencies in dopamine signaling in presymptomatic Huntington's disease mice. *Proc. Natl. Acad. Sci. USA* **97**, 6809–6814 (2000).
39. Vonsattel, J.P. Huntington disease models and human neuropathology: similarities and differences. *Acta Neuropathol.* **115**, 55–69 (2008).
40. Rudnicki, D.D., Pletnikova, O., Vonsattel, J.P., Ross, C.A. & Margolis, R.L. A comparison of huntington disease and huntington disease–like 2 neuropathology. *J. Neuropathol. Exp. Neurol.* **67**, 366–374 (2008).
41. Reinhart, P.H. *et al.* Identification of anti-inflammatory targets for Huntington's disease using a brain slice-based screening assay. *Neurobiol. Dis.* **43**, 248–256 (2011).
42. Slow, E.J. *et al.* Absence of behavioral abnormalities and neurodegeneration *in vivo* despite widespread neuronal huntingtin inclusions. *Proc. Natl. Acad. Sci. USA* **102**, 11402–11407 (2005).
43. Okamoto, S. *et al.* Balance between synaptic versus extrasynaptic NMDA receptor activity influences inclusions and neurotoxicity of mutant huntingtin. *Nat. Med.* **15**, 1407–1413 (2009).
44. Bodner, R.A. *et al.* Pharmacological promotion of inclusion formation: a therapeutic approach for Huntington's and Parkinson's diseases. *Proc. Natl. Acad. Sci. USA* **103**, 4246–4251 (2006).
45. Li, L., Murphy, T.H., Hayden, M.R. & Raymond, L.A. Enhanced striatal NR2B-containing *N*-methyl-d-aspartate receptor–mediated synaptic currents in a mouse model of Huntington disease. *J. Neurophysiol.* **92**, 2738–2746 (2004).
46. Murphy, K.P. *et al.* Abnormal synaptic plasticity and impaired spatial cognition in mice transgenic for exon 1 of the human Huntington's disease mutation. *J. Neurosci.* **20**, 5115–5123 (2000).
47. Usdin, M.T., Shelbourne, P.F., Myers, R.M. & Madison, D.V. Impaired synaptic plasticity in mice carrying the Huntington's disease mutation. *Hum. Mol. Genet.* **8**, 839–846 (1999).
48. Lynch, G. *et al.* Brain-derived neurotrophic factor restores synaptic plasticity in a knock-in mouse model of Huntington's disease. *J. Neurosci.* **27**, 4424–4434 (2007).
49. Starling, A.J. *et al.* Alterations in *N*-methyl-D-aspartate receptor sensitivity and magnesium blockade occur early in development in the R6/2 mouse model of Huntington's disease. *J. Neurosci. Res.* **82**, 377–386 (2005).
50. Hardingham, G.E. & Bading, H. Synaptic versus extrasynaptic NMDA receptor signalling: implications for neurodegenerative disorders. *Nat. Rev. Neurosci.* **11**, 682–696 (2010).
51. Cepeda, C., Wu, N., Andre, V.M., Cummings, D.M. & Levine, M.S. The corticostriatal pathway in Huntington's disease. *Prog. Neurobiol.* **81**, 253–271 (2007).
52. Nakanishi, N. *et al.* Neuroprotection by the NR3A subunit of the NMDA receptor. *J. Neurosci.* **29**, 5260–5265 (2009).
53. Hansson, O. *et al.* Transgenic mice expressing a Huntington's disease mutation are resistant to quinolinic acid–induced striatal excitotoxicity. *Proc. Natl. Acad. Sci. USA* **96**, 8727–8732 (1999).
54. Graham, R.K. *et al.* Differential susceptibility to excitotoxic stress in YAC128 mouse models of Huntington disease between initiation and progression of disease. *J. Neurosci.* **29**, 2193–2204 (2009).

ONLINE METHODS

DNA constructs. Expression plasmids encoding HTT^{ex1} or ataxin 1 variants fused to GFP were described previously[20,55]. HA-GluN1-1a was from T. Yamamoto, and HA-GluA1 was from M. Ehlers. HA-GluN3A was obtained by replacing the GFP tag in GFP-GluN3A[22]. Myc-tagged and mCherry-tagged rat PACSIN1 were cloned in pRK5. A 59-bp shRNA encoding a 19-bp specific sequence for rat and mouse PACSIN1 (shPACSIN1, target sequence CCATAGAGTTCCAGACATA) or a scrambled control shRNA (sh-SCR, GATCAGTGCCAACTTAACA) were cloned into pSuper-GFP vector (OligoEngine, Seattle, WA).

Cell culture and transfection. Primary striatal neuronal cultures were prepared from embryonic day 19 rat embryos[8] and transfected at day 8 *in vitro* using calcium phosphate. Experiments were performed 24–48 h later.

Immunofluorescence microscopy. For immunofluorescence analysis of the colocalization of endocytic proteins with HTT aggregates, HTT^{ex1}-GFP–transfected neurons were fixed with 4% sucrose and 4% paraformaldehyde in PBS, permeabilized with 0.1% saponin or Triton X-100, 1% BSA and 2% normal goat serum in PBS and incubated with primary antibodies followed by incubation with Cy3-conjugated secondary antibody (1:1,000, Jackson ImmunoResearch, 115-165-003). Mouse primary antibodies used were specific to PACSIN1 (1:200, 611811 (discontinued)), α-adaptin (1:500, 610501) and EEA1 (1:250, 610456) from BD Transduction Labs or to TfR (1:500, Invitrogen, 13-6800). The specificity of the antibody to PACSIN1 was tested by immunofluorescence in neurons transfected with two different PACSIN1 shRNAs. Images of HTT^{ex1}-GFP–transfected neurons were captured using a CoolSnap HQ camera (Photometrics) mounted on a Zeiss Axiovert 200 or a Zeiss LSM 510 confocal microscope using a ×63, 1.4 numerical aperture (NA) Plan-Apochromat objective. Colocalization was quantified using a custom-made ImageJ plug-in to apply the intensity correlation analysis of Li *et al.*[21]. Comparisons were made from pairs of single-image planes through the soma or individual dendritic fragments after background subtraction in each channel. Regions of interest (ROIs) containing aggregates were drawn in somatic regions of mHTT-transfected neurons, and fluorescence pixel intensities were quantified in matched ROIs in the green (GFP-HTT^{ex1}) and red (PACSIN1) channels. The difference from the mean for each pixel intensity (R_i–R_{mean} and G_i–G_{mean}, where R and G are the red and green pixel intensities) and the product of the differences (PDM = (R_i–R_{mean}) × (G_i–G_{mean})) were calculated. PDMs are positive when both the green and red pixel intensities vary in synchrony (that is, both the red and green pixel intensities are either above or below their respective means). An intensity correlation quotient (ICQ) was then calculated that is equal to the ratio of the number of positive PDM values to the total number of pixels. The ICQ ranges between −0.5 and 0.5 (with random staining, ICQ = 0; with dependent staining, 0 < ICQ < 0.5; and with segregated staining, 0 > ICQ > −0.5). Image sets were analyzed only in image regions that were free of pixel saturation, and pixel staining pairs with double zero-level intensity values were removed. Enrichment of PACSIN1 in aggregates was additionally quantified by comparing PACSIN1 fluorescence intensities in aggregates to intensities in nonaggregate ROIs (**Supplementary Fig. 1**). To quantify dendritic PACSIN1 expression in HTT^{ex1}-GFP–transfected neurons, all individual dendritic segments in the focus plane were outlined, and their average pixel intensities were normalized to the somatic intensity to obtain a dendrite-to-soma ratio for each transfected and untransfected neuron in the same field. For total PACSIN1 measurements, HTT^{ex1}-GFP–transfected neurons were outlined in the green channel and transferred to the red channel, and the average intensities measured after background subtraction were compared to those of untransfected neurons in the same field. Immunofluorescence analysis of surface receptor expression was as described[8]. Briefly, live transfected striatal neurons were incubated with an HA-specific antibody (1:200, Covance, MMS-101P) for 30 min at 37 °C, fixed and blocked, and surface HA receptors were detected with Cy3-conjugated secondary antibody. Neurons were then permeabilized, and internal HA receptors were labeled with HA-specific antibody and detected with Alexa Fluor 647 secondary antibody (1:200, Invitrogen, A21235). Wide-field fluorescence images were acquired with a Zeiss ×40 or ×63 objective and a CoolSnap charge-coupled device (CCD) camera and analyzed with MetaMorph. For quantification, neurons were outlined in the GFP channel, and the outlines were transferred to the red and far-red channel images to obtain average intensity measurements. Surface-to-internal ratios were calculated by dividing the Cy3 intensity values by the Alexa Fluor 647 intensity values.

Transferrin (Tf) uptake assay. Striatal neurons were incubated with Alexa Fluor 568–conjugated Tf (50 μg ml^{-1}) in serum-free medium for 10 min at 37 °C. Cells were then washed with serum-free medium at 10 °C and incubated with holotransferrin (500 μg ml^{-1}) in conditioned medium to exchange the surface-bound Tf and selectively monitor the endocytosed fraction. After washing, neurons were fixed, and remaining intracellular Alexa-Tf was imaged. For quantification, fluorescent intensities of Alexa-Tf within three to four 50-μm dendritic segments of HTT^{ex1}-GFP–transfected neurons were measured for each neuron, averaged and normalized to the Tf uptake values of untransfected neurons in the same field.

RNA interference. HEK293 cells transfected with Myc-PACSIN1 and control or PACSIN1-specific shRNAs were lysed, and PACSIN1 expression was analyzed by immunoblotting with a Myc-specific antibody (1:1,000, Invitrogen, clone 9E10) and normalizing to the GFP band (1:5,000, Clontech, clone JL-8). shPACSIN1 was additionally tested in striatal neurons by transfection with calcium phosphate and quantification of total endogenous PACSIN1 expression.

Human postmortem brain tissue. Samples of putamen from humans with Huntington's disease and controls were obtained from Banc de Teixits Neurològics (Servei Científico-Tècnics, Universitat de Barcelona, Spain) following the ethical guidelines of the Declaration of Helsinki. Case information can be found in **Supplementary Table 1**. Informed consent was obtained from all subjects under study. GluN3A expression was analyzed in postnuclear supernatants by western blotting as described below. A rabbit antibody generated against a fragment of mouse GluN3A expanding amino acids 1041–1152 was used[34]; the specificity of the human GluN3A band was assessed by comparison with a mouse GluN3A band that was absent in GluN3A knockout mice and was run in parallel in the same blot.

Transgenic mice. Three Huntington's disease models were used in this study: transgenic R6/1 mice expressing exon 1 of human *HTT* carrying 115 CAG repeats[27], YAC128 mice (line 55 homozygotes) containing full-length human *HTT* with 128 CAG repeats[19] and Hdh^{Q111} mice, with targeted insertion of a 109 CAG repeat in the murine *Hdh* locus that extends the glutamine segment in mouse HTT to 111 residues[56]. $Hdh^{Q7/Q111}$ heterozygous males and females were intercrossed to generate $Hdh^{Q7/Q111}$ heterozygous and $Hdh^{Q7/Q7}$ control littermates. Age-matched and genetic background–matched wild-type mice were used as controls for the biochemical analyses in **Figure 3** and **Supplementary Figures 5** and **6** and for the initial spine analysis in **Supplementary Figure 7** (CBA × C57BL/6 littermates for R6/1 mice, FVB/N mice for YAC128 mice and $Hdh^{Q7/Q7}$ littermates for $Hdh^{Q7/Q111}$ mice). Transgenic mice with juvenile GluN3A expression levels through adulthood[16] (double-transgenic GFP-GluN3A) and single-transgenic littermates were used in spine-density and neuropathological analyses. For rescue experiments, YAC128 mice (in a FVB/N background) were crossed to $Grin3a^{-/-}$ mice[15] (in a C57BL/6 background), yielding heterozygous mice that were then crossed to obtain wild-type, $Grin3a^{-/-}$, YAC128 and YAC128 × $Grin3a^{-/-}$ mice. Littermate offspring from both sexes were used unless otherwise indicated. Electrophysiological, spine and neuropathological experiments were replicated in several mouse cohorts to minimize potential confounding effects of genetic background, and in all cases experimenters were blind to the genotype of the mice until analysis was completed. All procedures conformed to the European Community guidelines for the care and use of laboratory animals and were approved by the Ethical Committee of the University of Navarra (in accord with the Spanish Royal Decree 1201/2005).

Biochemistry. For immunoprecipitation experiments, striatal tissue or transfected HEK293 cells were lysed in T-PER buffer (Pierce) supplemented with protease inhibitors (Roche Applied Science). Protein concentrations were measured using a bicinchoninic acid (BCA) kit (Pierce). After preclearing, lysates were incubated with a GFP-specific antibody (1:500, Synaptic Systems,

132002), a monoclonal antibody to HTT (1:500, Millipore, MAB2166) or ImmunoPure Rabbit or Mouse Gamma Globulin (Thermo Scientific) for 4 h at 4 °C. Antibody-bound proteins were separated by centrifugation after 2 h of incubation with protein A/G agarose beads (Pierce), washed extensively with T-PER buffer, eluted with sample buffer (Bio-Rad), resolved using Criterion XT 3–8% Tris-acetate precast gels (Bio-Rad) and analyzed by immunoblotting using antibodies to PACSIN1 (1:1,000, Synaptic Systems, 196-0P), GFP (1:5,000, Clontech, JL-8) or HTT (1:1,000, Sigma, H7540).

Total plasma membranes or SPMs from mouse striatal tissue were obtained by biochemical fractionation as described[8]. Further detergent extraction of striatal synaptic plasma membranes to yield an insoluble PSD-enriched fraction and a soluble non–PSD enriched fraction (which includes perisynaptic and extrasynaptic receptors) was conducted using the protocol described by Milnerwood *et al.*[13]. Protein samples were resolved by SDS-PAGE, transferred onto polyvinylidene fluoride (PVDF) membranes and detected by immunoblot (ECL Plus, Amersham) using antibodies to GluN1 (1:2,000, MAB363), synaptophysin (1:20,000, MAB5258), GluN2A (1:500, 07-632) and GluA2 and GluA3 (GluA2/3) (1:1,000, 07-598) purchased from Millipore and antibodies to GluN2B (1:200, NeuroMab, N59/20), GluN3A (1:1,000, ref. 34), PACSIN1 (1:1,000, Synaptic Systems, 196-0P), Rab4 (1:1,000, Enzo Life Sciences, ADI-KAP-GF005), Rab11 (1:1,000, BD Transduction Labs, 610657) and DARPP32 (1:1,000, BD Transduction Labs, 611520). Band intensities were quantified on a phosphorimager (Storm 860, Amersham) using Image-Quant 5.0 software or on a GS-800 calibrated densitometer (Bio-Rad).

Surface cross-linking. To analyze the expression of glutamate receptor subunits in the intracellular pool, we used the membrane-impermeable cross-linker BS3 (Pierce) as described previously[57]. Acute corticostriatal slices (270 µm thick) from age-matched YAC128 and FVB/N mice were allowed to recover for 45 min in Krebs buffer. Slices were then incubated for 30 min at room temperature in freshly prepared BS3 (1 mg ml^{-1} in Dulbecco's PBS (D-PBS)) or D-PBS. A minimum of three slices per control or treatment group were included for each mouse. To quench the remaining BS3, slices were washed three times in cold 0.1 M glycine in D-PBS and then in D-PBS. Striata were then dissected out and lysed in 0.32 M sucrose and 4 mM 4-(2-hydroxyethyl)-1-piperazineethanesulfonic acid (HEPES) with protease inhibitors (Roche) and PMSF (Sigma). The content of the intracellular pool of receptors was determined by western blotting (cross-linked surface receptor complexes are retained in the stacking gel) and normalized to the total receptor (nontreated).

Brain immunohistochemistry. Mice were deeply anesthesized and perfused intracardially with 4% paraformaldehyde in 0.1 M phosphate buffer (pH 7.4). Coronal brain sections (30 µm) were cut with a freezing sliding microtome and stained with antibodies to GluN3A (1:100), DARPP32 (1:1,000) and NeuN (1:100, Millipore, MAB377). Antigen-retrieval techniques were required to reveal endogenous GluN3A. GluN3A immunoreactivity was absent from the brains of *Grin3a*$^{-/-}$ mice, establishing the specificity of the antibody for immunohistochemistry. Binding of the primary antibody was visualized using the appropriate biotin-conjugated secondary antibody (1:200, Thermo Scientific, 32052 or 32054) followed by an ABC kit (Pierce) and diaminobenzidine and H_2O_2 or with Alexa Fluor 488 anti-Rabbit (1:300, Jackson Immunoresearch, 711-545-152) and Alexa Fluor 555 anti-Mouse (1:1,000, Invitrogen, A21424).

For stereological analysis, unbiased counting relative to genotype and condition was performed using the Computer Assisted Stereology Toolbox (CAST) software (Olympus Danmark) as described[58]. Briefly, striatal volume was obtained by the Cavalieri method. For counts of DARPP-32–positive and NeuN-positive neurons per striatum, we used the dissector-counting procedure in coronal sections that were 30-µm thick and spaced 240 µm apart. For estimating the mean cellular and perikaryal volumes of neurons (the so called 'local volumes') with design-based stereology, the 'nucleator' method was used.

Real-time quantitative PCR. Total RNA from mouse striatum was isolated using TRIzol Reagent (Life Technologies). First-strand cDNA was synthesized from 1 µg of total RNA starting material using the Superscript III First-Strand Synthesis System for RT-PCR (Invitrogen). Quantitative real-time PCR (qPCR) was performed using a predesigned TaqMan Gene Expression assay kit (Applied Biosystems) consisting of a pair of unlabeled forward and reverse amplification primers and a TaqMan probe with a FAM dye label. Briefly, real-time qPCR was assayed in a total volume of 25 µl reaction mixture containing 5 µl of diluted cDNA, 12.5 µl of 2× TaqMan Universal Master Mix, 1.25 µl of the 20× TaqMan Gene Expression Assay and RNase-free water. Taqman probes for GluN3A (Mm 01341719_m1) and glyceraldehyde-3-phosphate dehydrogenase (GAPDH) (Mm 99999915_g1) were from Applied Biosystems. Probe Mm 01341719_m1 recognizes exons 2–3 of the mouse *Grin3a* gene. PCR thermal conditions included an initial 10 min at 95 °C followed by 40 cycles of denaturation for 15 s at 95 °C and annealing and primer elongation for 1 min at 60 °C. All qPCR reactions were run in triplicate in two independent experiments using the Applied Biosystems 7300 RT-PCR system. Mean cycle threshold (Ct) values for each reaction were recorded for posterior data analyses. The relative RNA expression levels were calculated using GAPDH as a control: $\Delta Ct = Ct_{GAPDH} - Ct_{GluN3A}$. The gene expression fold change, normalized to GAPDH and relative to the control sample, was calculated as $2^{\Delta Ct}$.

Electrophysiology. The methods described for **Figure 1** of ref. 13 were followed almost exactly except that the tip diameter of the stimulating electrode was larger (~20 µm) and the stimulus duration was 200 µs. The distance from the stimulating to the recording electrode was approximately 175 µm. The temperature was 23–25 °C. The intracellular solution contained (in mM) 140 Cs-gluconate, 9 NaCl, 1 $MgCl_2$, 0.2 $CaCl_2$, 1 ethylene glycol tetraacetic acid (EGTA), 10 HEPES, 2 MgATP, 0.2 LiGTP and 5 Qx314, and the extracellular solution contained (in mM) 120 NaCl, 2.5 KCl, 2 $CaCl_2$, 10 glucose, 1.25 NaH_2PO_4, 26 $NaHCO_3$, nominally 5 µM $MgCl_2$, 20 µM glycine, 2 µM strychnine, 50 µM picrotoxin and 50 µM D-(−)-AP5 when indicated. Mice were 28- to 35-day-old males, and experimenters were blind to genotype. The same results were obtained in two independent mice cohorts.

Golgi impregnation and spine quantification. Fresh brain hemispheres were processed following the Golgi-Cox method[59]. The slides were randomly coded, and the experimenter was blind to genotype during image acquisition and analysis. Bright-field images of Golgi-impregnated striatal MSNs were captured with a Nikon DXM 1200F digital camera attached to a Nikon Eclipse E600 light microscope (×100 oil objective). Only fully impregnated MSNs with their soma found entirely within the thickness of the section and with at least four orders of dendrites visible were considered for analysis. Image *z* stacks were taken every 0.5 µm and analyzed with ImageJ. Dendritic segments (>20-µm long; average, 47.35 µm; mean range, 20–95 µm) were traced through different layers of the stack, and the spines were counted. Spine density was calculated in four to eight dendrites of each order per neuron, and the values were averaged to obtain neuronal averages.

Electron microscopy. For electron microscopy, mice were anesthetized and perfused with saline, followed by 4% paraformaldehyde and 1.5% glutaraldehyde in phosphate buffer. Coronal sections were then cut at a thickness of 60 µm using a Leica vibration microtome through the striatum. After several washes in phosphate buffer, sections were postfixed with osmium tetraoxide (1% in phosphate buffer) and block stained with uranyl acetate (1% in distilled water). Sections were then dehydrated, treated with propylene oxide and flat embedded on glass slides in Durcupan (Fluka). Striata were cut at 70 nm on an ultramicrotome (Reichert Ultracut E, Leica) and collected on 200 mesh copper grids. Staining was performed on drops of 1% aqueous uranyl acetate followed by Reynolds's lead citrate. Ultrastructural analyses were performed in a Jeol-1010 electron microscope. For analysis of synapse number and size, the dissector principle was applied, and 15 fields of 64.392 µm^2 at the striatum of each mouse were randomly acquired and analyzed in a blind fashion.

Behavioral characterization. Two independent mouse cohorts, each containing mice from four genotypes (wild-type, *Grin3a*$^{-/-}$, YAC128 and YAC128 × *Grin3a*$^{-/-}$), were used. Cohort 1 was used for motor and open-field assessment and included 10-month-old male mice. Cohort 2, used for testing cognitive function, included 12-month-old mice of both sexes. Body weight, muscular strength and open-field activity were measured[29]. For rotarod learning assessment, mice were trained at a fixed speed of 10 r.p.m. and subsequently tested

doi:10.1038/nm.3246

with two trials per day spaced 1–2 h apart during 3 consecutive days. During this learning phase, mice falling from the rod were returned, and the number of falls was recorded until the addition of the latencies to fall reached a total time of 60 s per trial[13,29]. For the accelerating task, the rotarod was accelerated from 5 to 40 r.p.m. over 5 min. The latency to fall was recorded for each of two trials and averaged. For the vertical pole test, a metal pole (1.5 cm in diameter, 50 cm long) wrapped with cloth tape was used. The mouse was placed in the center of the pole, which was held in a horizontal position. The pole was then gradually lifted to a vertical position, and the latency to fall was measured. For the swimming T-maze test, a T maze (dimensions: arms, 38 × 14 cm; platform, 10 × 14 cm) was filled with water to a depth of 7 cm, and a submerged escape platform was located in the right arm of the maze. Mice were placed into the water at the base of the stem arm of the maze and learned the location of the escape platform. During the normal testing phase, mice received four trials per day spaced 45 min apart for 3 consecutive days. For reversal learning, the platform was switched to the left arm of the maze. Mice received four trials spaced 45 min apart. Times to reach the hidden platform were recorded.

HTT exon 1 brain-slice assay. Brain-slice assays for $HTT^{ex1}Q73$-induced neurodegeneration were as described[41]. Briefly, 250-μm thick corticostriatal brain slices from P10 Sprague-Dawley rat pups of both sexes were prepared on a vibratome and placed in an interface configuration over culture medium containing 15% heat-inactivated horse serum, 10 mM KCl, 10 mM HEPES, 100 U ml^{-1} penicillin and streptomycin, 1 mM sodium pyruvate and 1 mM L-glutamine in Neurobasal A (Invitrogen) under 5% CO_2 at 32 °C. Rat pups were euthanized in accordance with US National Institutes of Health guidelines and under Duke University Medical Center Institutional Animal Care and Use Committee approval. Slices were biolistically transfected (Helios gene gun, Bio-Rad) with DNA plasmids encoding YFP, $HTT^{ex1}Q73$, and/or GluN3A, all in gWiz (Genlantis). Four days after transfection, MSNs were identified by their location within the striatum and by their characteristic dendritic arborization and scored as healthy if they showed continuous YFP fluorescence throughout a cell body of normal diameter and at least two clear and unbroken primary dendrites that were at least two cell body–diameters long.

Statistics. Values are shown as the mean ± s.e.m. Student's *t* test was used for simple comparisons of one variable between two groups, and one- or two-way ANOVA followed by Bonferroni or Tukey *post hoc* tests were used to determine differences between more than two groups, unless otherwise indicated in the figure legends. The level of statistical significance was set at $P < 0.05$. No statistical method was used to predetermine sample size, and the animal experiments were not randomized.

55. Irwin, S. *et al.* RNA association and nucleocytoplasmic shuttling by ataxin-1. *J. Cell Sci.* **118**, 233–242 (2005).
56. Lloret, A. *et al.* Genetic background modifies nuclear mutant huntingtin accumulation and HD CAG repeat instability in Huntington's disease knock-in mice. *Hum. Mol. Genet.* **15**, 2015–2024 (2006).
57. Grosshans, D.R., Clayton, D.A., Coultrap, S.J. & Browning, M.D. Analysis of glutamate receptor surface expression in acute hippocampal slices. *Sci. STKE* **2002**, PI8 (2002).
58. Giralt, A., Carreton, O., Lao-Peregrin, C., Martin, E.D. & Alberch, J. Conditional BDNF release under pathological conditions improves Huntington's disease pathology by delaying neuronal dysfunction. *Mol. Neurodegener.* **6**, 71 (2011).
59. Ricobaraza, A., Cuadrado-Tejedor, M., Marco, S., Perez-Otano, I. & Garcia-Osta, A. Phenylbutyrate rescues dendritic spine loss associated with memory deficits in a mouse model of Alzheimer disease. *Hippocampus* **22**, 1040–1050 (2012).